HHS Public Access

Author manuscript

NMR Biomed. Author manuscript; available in PMC 2020 October 01.

Published in final edited form as:

NMR Biomed. 2019 October ; 32(10): e3962. doi:10.1002/nbm.3962.

Assessing High-Intensity Focused Ultrasound Treatment of Prostate Cancer with Hyperpolarized ^{13}C Dual-Agent Imaging of Metabolism and Perfusion

Jessie E. Lee[1,2], **Chris J. Diederich**[1,2,3], **Robert Bok**[1], **Renuka Sriram**[1], **Romelyn Delos Santos**[1], **Susan M. Noworolski**[1,2], **Vasant A. Salgaonkar**[3], **Matthew S. Adams**[2,3], **Daniel B. Vigneron**[1,2], **John Kurhanewicz**[1,2]

[1]Department of Radiology and Biomedical Imaging, University of California, San Francisco

[2]University of California, Berkeley, and University of California, San Francisco Joint Graduate Program in Bioengineering

[3]Department of Radiation Oncology, University of California, San Francisco

Abstract

The goal of the study was to establish early hyperpolarized ^{13}C MRI metabolic and perfusion changes that predict effective high-intensity focused ultrasound ablation and lead to improved adjuvant treatment of partially treated regions. To accomplish this a combined hyperpolarized (HP) dual agent (^{13}C-pyruvate and ^{13}C-urea) ^{13}C MRI/mp-^{1}H MRI approach was used to measure prostate cancer metabolism and perfusion 3–4 hours, 1 day and 5 days after exposure to ablative and sub-lethal doses of HIFU within adenocarcinoma of mouse prostate (TRAMP) tumors using a focused ultrasound applicator designed for murine studies. Pathologic and immunohistochemical analysis of the ablated tumor demonstrated fragmented, non-viable cells and vasculature consistent with coagulative necrosis, and a mixture of destroyed tissue and highly proliferative, poorly differentiated tumor cells in tumor tissues exposed to sub-lethal heat doses in the ablative margin. In ablated regions, the intensity of HP ^{13}C lactate or HP ^{13}C urea and DCE MRI AUC images were reduced to the level of background noise by 3 to 4 hours after treatment with no recovery by the 5-day time point in either case. In the tissues that received sub-lethal heat dose, there was a significant 60% ± 12.4% drop in HP ^{13}C lactate production and a significant 30 ± 13.7% drop in urea perfusion 3–4 hours after treatment, followed by recovery back to baseline by 5 days after treatment. DCE MRI K^{trans} showed a similar trend as HP ^{13}C urea, demonstrating a complete loss of perfusion with no recovery in the ablated region while having a 40%–50% decrease 3–4 hours after treatment followed by recovery to baseline values by 5 days. The utility of the HP ^{13}C MR measures of perfusion and metabolism in optimizing focal HIFU, either alone or in combination with adjuvant therapy, deserves further testing in future studies.

Graphical Abstract

Corresponding author: John Kurhanewicz, Professor Depts. of Radiology and Biomedical Imaging, Urology and Pharmaceutical Chemistry, Member of the UCSF/UCB Joint Bioengineering Graduate Program and UCSF Cancer Center, Director of the Prostate Imaging Group and Biomedical NMR Laboratory, University of California San Francisco, 1700 Fourth Street, Byers Hall Room BH203, San Francisco, CA 94158, John.Kurhanewicz@radiology.ucsf.edu.

Mice with prostate tumors were treated with HIFU, resulting in partial ablations within the tumors. In a single MRI acquisition after the injection of copolarized [1-^{13}C]pyruvate and ^{13}C-urea, the region of HIFU-induced coagulative ablation can be identified by a complete loss of perfusion and metabolism. The recovery of perfusion and metabolism over-time in surrounding tissues that received non-lethal hyperthermic heat doses could be used to identify the best time to apply adjuvant chemo- and radiation therapy.

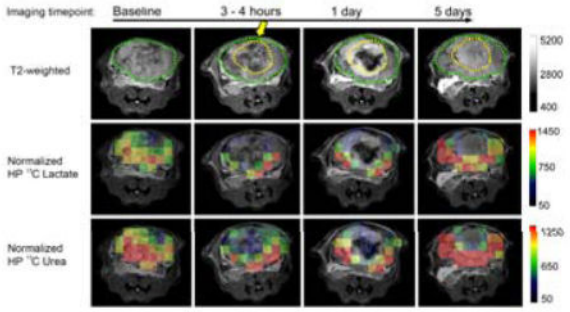

Keywords

Prostate cancer; pyruvate metabolism; urea perfusion; hyperpolarized ^{13}C MRI; HIFU

Introduction

Prostate cancer is the most frequently diagnosed invasive cancer in men.[1] However, prostate cancer is extremely variable in its aggressiveness and subsequent history of progression to a lethal disease.[1] Men diagnosed with low- or intermediate-risk localized prostate cancer have historically faced the dilemma of having to select either aggressive definitive treatments such as surgery or whole-gland radiation therapy with their associated complications, or the psychologically burdensome option of active surveillance without treatment.[2,3] Focal therapies have recently been integrated within the clinic that allow for definitive treatment of low- or intermediate-risk intraprostatic lesions while reducing the risk of significant complications seen with more radical therapy.[4–7] High-intensity focused ultrasound (HIFU) is one of the modalities being investigated as a precision technique for effective thermal ablation for such cases.[7–9]

HIFU or Focused Ultrasound (FUS) is capable of creating ablative levels of tissue heating within tumor via delivery of ultrasound energy while sparing structures outside of the beam focus.[10] Responses of tissues to thermal therapies depend on both the temperature elevation and the duration. In general, high-intensity ultrasound refers to ultrasound with intensity greater than 5W/cm^2.[11] Immediate cell death occurs at a temperature beyond 56°C for at least 1 second.[12] During HIFU treatment, a high-power ultrasound wave is focused at the focal point, raising the temperature in the focal zone to beyond 80°C within seconds.[13] This heat exposure leads to protein denaturation, mitochondrial dysfunction, irreversible cell death, and coagulative necrosis in the ablated zone.[13,14] In the margin zone (the zone directly adjacent to the ablated zone), a mixture of destroyed tissue and viable cells is observed. The tissues in the margin zone still receive thermal-induced injuries, but the

effects can be sub-lethal and reversible.[14] Some of the cells damaged with primary thermal insult will undergo partial cellular breakdown and subsequent recovery.[15] Other cells will die subsequently due to secondary injury (inflammation, apoptosis, ischemia, etc.).[15]

Image guidance, provided by ultrasound or MRI, is crucial in improving tissue targeting and treatment monitoring, and promising results have been shown in various applications in clinical trials.[16–24] The superior soft-tissue contrast and high spatial-resolution make MRI the best imaging method for prostate cancer.[25] The current state-of-the-art for imaging localized prostate cancer, multiparametric (mp) ^{1}H MRI (anatomic, perfusion and diffusion weighted imaging), has demonstrated the ability to localize tumors for subsequent biopsy and focal treatment.[25] In addition, with the ability to provide real-time thermometry feedback, MRI allows for even better controlled heat deposition.[26,27] Therefore, the combination of HIFU and MR-guidance is a powerful focal therapy modality for localized prostate cancer.[5,28–31] While there are multiple ways to assess treatment outcome, including ultrasound-measured elasticity and the clinical gold standard dynamic contrast-enhanced (DCE) MRI, these methods only delineate coagulated tissues or the lack of perfusion.[32,33]. There remains a clinical need to define effective ablation at an earlier time point and provide critical metabolic and perfusion information on the partially treated regions for improved adjuvant therapy.

Varying heat doses in partially treated regions may cause a diverse effect on residual areas of prostate cancer perfusion and metabolism, which could hold the key to more accurately assessing treatment response at an early time-point and for improving treatment protocols for individual patients. Hyperpolarized ^{13}C MRI is a powerful new metabolic imaging method which uses specialized instrumentation to provide signal enhancements of over 10,000-fold for ^{13}C enriched, safe, endogenous, non-radioactive compounds. The unprecedented gain in sensitivity provided by hyperpolarization can be combined with fast ^{13}C MRI techniques to provide high-spatial resolution images of the injected metabolic probe, HP [1-^{13}C] pyruvate, as well as its down-stream metabolites.[34] Specifically the apparent rate of conversion of HP [1-^{13}C] pyruvate to [1-^{13}C] lactate (k_{PL}) catalyzed by lactate dehydrogenase (LDH) and the associated HP [1-^{13}C] lactate/[1-^{13}C] pyruvate ratio and has shown great potential for not only detecting prostate cancer, but for also assessing the aggressiveness (pathologic grade) of the cancer and its subsequent response to therapy in both pre-clinical and clinical studies.[34–39] Prostate cancer, particularly high-grade prostate cancer, is associated with a high HP [1-^{13}C] lactate/[1-^{13}C] pyruvate ratio and k_{PL} and both are dramatically reduced with effective treatment.

Another important feature of HP ^{13}C MRI is that it can encode chemical as well as spatial information, thereby providing the potential for using multiple HP ^{13}C-labeled probes in order to detect both metabolism ([1-^{13}C] pyruvate) and perfusion (^{13}C-urea) simultaneously after a single injection of the combined HP probes.[25,40] Initial pre-clinical studies have indicated that metabolically inactive [^{13}C] urea can be used as a perfusion contrast agent to image blood flow, and has several advantages over gadolinium-based agents, including direct proportionality of signal to tracer concentration, naturally substance at physiologic concentrations and inherently high contrast-to-noise ratio due to the absence of background signal.[40] As mentioned above, DCE MRI currently serves as the clinical gold standard of

assessing HIFU treatment efficacy, and in this study the serial HP ^{13}C-urea change after HIFU was compared to DCE MRI to assess whether it provides similar or improved information. Methods for co-polarizing ^{13}C-pyruvate and ^{13}C-urea have also been developed, successfully polarized, and injected in pre-clinical models to simultaneously measure perfusion and metabolism.[40] In a recent dual probe (^{13}C urea and [1-^{13}C] pyruvate) HP ^{13}C MRI pre-clinical study of prostate cancer, significant changes in ^{13}C-urea (perfusion) was able to distinguish high- from low-grade cancer.[37] Currently, there is no published data on the temporal changes in perfusion and glycolytic metabolism that occur with complete ablation or partially HIFU treated tissues.

In this study a combined HP dual agent (^{13}C-pyruvate and ^{13}C-urea) ^{13}C MRI/mp-^{1}H MRI approach was used to characterize temporal changes in prostate cancer metabolism and perfusion after exposure to ablative and sub-lethal doses of HIFU using a transgenic adenocarcinoma of mouse prostate (TRAMP) model [41,42] and a focused ultrasound applicator designed for murine studies. The overall goal of the study is to establish early HP ^{13}C MRI metabolic and perfusion changes that predict effective HIFU treatment and lead to improved adjuvant treatment of partially treated regions.

Material and Methods

Murine Tumor Model

The TRAMP model is a well-established murine prostate model that closely mimics the progression of human prostate cancer.[41,42] Specifically, the perfusion and metabolism of TRAMP model mimic human disease.[37,43] Mice of C57Bl6 X FVB background, (n=5) weighing 30–40g with solid prostate tumor of 1.5–2.2 cm^3 were selected for HIFU treatments (Table 1). Tumor size was determined by identifying the tumor region of interests (ROIs) on the T2-weighted anatomical MRI images. During the HIFU treatment and the MRI session, mice were anesthetized with 1%-2% isoflurane. A pressure sensor (SA Instruments, NY, USA) for respiration monitoring was placed under the animal, positioned within the mouse holder and the coil that fit in the 14T MRI scanner. The respiration rate was maintained at 60–75 breaths/minute.

Small Animal FUS Device—Fabrication and Characterization

Small focused ultrasound applicators were fabricated in-house, using spherical focused transducers (PZT-4 material, 12.7mm diameter, 41.4mm radius of curvature, 5.6MHz) mounted on a 3D-printed acrylonitrile butadiene styrene (ABS) housing designed to provide air backing, conduits for RF power leads, and fluid injection port. This configuration was selected based upon practical constraints of size, frequency, and availability to provide a defined region of ablation within these mouse tumors, and not a small discrete focal zone. The transducer housing was integrated with a conical shaped standoff with a 1-cm diameter window, and filled with degassed water in order to couple the acoustic energy to the mouse and to adjust the distance such that the focus was within the tumor. The custom applicators were characterized and calibrated with intensity beam plots using a 3D computer controlled scanning system (Velmex Inc., Bloomfield, NY) with a calibrated hydrophone (HNP-0400, Onda Corp, Sunnyvale, CA). Applicators under test were operated in burst mode at 200

cycles with 1kHz repetition following standard measurement methods, and the peak-to-peak voltage from the hydrophone was measured using an oscilloscope (Keysight DSO-X-2024A 200MHz Digital Oscilloscope, Keysight Technologies, Santa Rosa, CA) and converted to intensity. Maps of the distribution and the peak intensity for applied powers were measured in degassed water. Intensity beam plots of the X–Z (coronal) and X–Y (axial) planes were acquired. The step sizes were 0.2mm along the X and Z axes and 1mm along the Y axis. The acoustic output power as a function of electrical input power (2W-16W) was measured using the radiation force balance technique, and used to scale applied power for desired high intensity delivery during animal studies.

FUS Tumor Ablation

The ventral and dorsal abdominal regions of the mouse around the tumor was depilated for efficient coupling of the ultrasound energy, and the applicator tip was placed and compressed over either left or right side of the tumor target region and coupled to the skin with ultrasound transmission gel. The applicator was positioned from a ventral-lateral approach so that no major organs were in the ultrasound beam path to avoid injuries in other organs. A 30 durometer rubber absorber and intermediate gel pad, with acoustic gel was positioned on the opposite side of the tumor to absorb and dissipate the exiting ultrasound energy, and to prevent reflection. RF power was applied continuous wave using a single channel from a four-channel amplifier (Advanced Surgical Systems, Inc.; 500-009 RF generator), and the sonications were performed at 5.6 MHz, 11.6–15W net electrical power, spatial-peak temporal-average intensity (I_{SPTA}) = 292.9–401.9W/cm^2 for 45 to 60 seconds. Each mouse received 1 to 2 treatments depending on the size of the tumor. The goal was to generate ablated and partially treated regions within the same TRAMP tumor for serial imaging studies, not to ablate the entire tumor or a specific discrete region for assessment of therapeutic efficacy. Therefore, ablative ultrasound intensities were directed toward one side or half of the tumor. A high-intensity and long-duration (60s) HIFU treatment was performed on Mouse 1, and then the power setting and duration were adjusted for the following mice to achieve optimal outcomes. For the subsequent mice, two sonications were performed for each mouse at a lower power and a shorter duration. Between the two sonications, the location of the applicator was shifted slightly (~1mm) in order to generate a larger thermal damage zone. Figure 1 shows the setup schema during a HIFU treatment. Table 1 lists the HIFU treatment parameters applied for TRAMP mice of varying tumor size and baseline metabolic activity that were studied. Both the HIFU intensity and duration were also varied between mice to allow for differing ablated and partially treated regions.

MR Imaging

The MR imaging was performed on a wide-bore 14T micro-imaging system (Varian Instruments, Palo Alto, CA) equipped with 1000 mT/m gradients and multi-nuclear capabilities. Each imaging study included (1) T_2-weighted images for anatomical references (TE/TR = 20/1200 ms; voxel size 0.16×0.16×1 mm^3, field of view 4cm × 4cm), (2) diffusion-weighted imaging (DWI) using a spin-echo diffusion weighted sequence (TE/TR = 20/1200ms; voxel size 0.31×0.31×1mm^3, field of view 4cm × 4cm, diffusion gradient amplitude 39G/cm, gradient duration 2ms, gradient separation 13ms, four b-values were used: 25, 188, 331, and 514s/mm^2), (3) DCE MRI acquired using a T1-weighted gradient

echo sequence serving as a comparison to the clinical standard (TE/TR = 1.11/39 ms; voxel size 0.31×0.31×1 mm; acquired over 5 minutes), and (4) the co-hyperpolarized [1-^{13}C] pyruvate and ^{13}C urea (voxel size 2.5×2.5×2.5 mm). The contrast agent gadolinium solution used for DCE MRI was made with Magnevist© at 1:6 dilution. A volume of 150μL of the gadolinium solution was injected through the tail vein catheter followed by 150μL flushing saline solution over a total of 30 seconds. The [1-^{13}C] pyruvate and ^{13}C urea samples, as well as the buffer solution, were prepared following the previously published protocols.[35,44] Once the samples were polarized, a dissolution step brought the samples back to physiologic temperature, and 450μL of the solution was injected through the tail vein catheter over 15 seconds. As determined in the previous studies, the ^{13}C images were acquired 35 seconds after the injection.[35] The ^{13}C data were acquired in the following order: (1) a 2-degree flip angle spectrum, (2) the 3D images of pyruvate, lactate, and urea using a 3D GRASE sequence,[45] and (3) a 90-degree flip angle spectrum. The spectra served as a supplemental verification of proper polarization levels and successful injections. These imaging studies were performed at four time points and comprise a baseline acquired 1 day before the treatment, 3–4 hours after the HIFU treatment, and both 1 and 5 days post-treatment.

Histopathology

Mice were sacrificed immediately after the last imaging time point, and the resected tumors were sliced in 3-mm sections and immersed in a freshly prepared solution of 2% (w/v) triphenyl tetrazolium chloride (TTC) in phosphate-buffered saline (PBS) for 25 minutes at room temperature. TTC is a tissue viability stain.[46] Functional dehydrogenases and cofactors convert the colorless TTC into a bright red pigment, while the non-viable tissues stay in the native color. Pictures of gross pathology were taken before and 25 minutes after the TTC staining. The tissues were then fixed in 10% buffered formalin, transitioned into ethanol, and embedded in paraffin blocks. The sliced tissues underwent standard histological processing and H&E staining, and sections were registered to the corresponding MR images. Based on the pathology, an investigator (RB) highly experienced in murine pathology identified two types of treated tissues as a result of different heat exposures: (1) complete ablation: regions not stained by TTC (appeared as the native tissue color) that had less than 10% viable, intact structures on H&E, (2) margin zone: regions with a weaker TTC staining that had less than 50% necrosis/fibrosis/coagulation on H&E, and (3) non-lethal exposure or untreated tumor tissues: regions with dark red TTC staining and appeared viable on H&E. The identified regions were correlated to the T2-weighted, HP ^{13}C, and DCE MRI results.

Data Analysis

The MR apparent diffusion coefficient (ADC) maps were calculated from the diffusion-weighted images using VNMRJ 4.0 (Agilent Inc., Santa Clara, CA, USA). The ablated and margin zones were identified on the T2-weighted, ADC, and DCE MRI images and verified with histopathology. These regions of interest (ROI) were drawn on the DCE MRI data using the Editor module in Slicer3 (http://www.slicer.org).[47] The means of the ROI's were calculated using LabelStatistics under the Quantification module. The same regions were then identified on the T2-weighted anatomical images and then overlapped onto the ^{13}C images using custom software developed in-house programmed in IDL Software.

Pharmacokinetic modeling was applied to the intensity-over-time DCE MRI data, based on the extended Tofts Kermode model using a native T1 = 1.4s and a relaxivity, r_1 = 3.7L/(mmol × s), and v_p = 0.1.[48] The arterial input function (C_p) was characterized using a bi-exponential function, based upon a study performed in mice, where $C_p(t) = Amp \times D(a_1 \exp\{(t - t_0)m_1\}) + a_2 \exp\{(t - t_0)m_2\})$, and where Amp = 20, D = 0.62 mmol/kg of Gd-DTPA, a_1 = 0.1 kg/L, m_1 = 0.0175/min, a_2 = 0.19 kg/L, m_2 = 0.00115/min.[49] The Amp was introduced to account for overall signal differences between our experimental measures and the one from the literature, and as only measures normalized to pre-treatment values were reported. The model was fit to the data using non-linear least squares estimation with the "optim" function in R (R Foundation for Statistical Computing, Vienna, Austria).[50] The quantitative DCE transfer constants (K^{trans}) were computed, and the values were normalized to the baseline values prior to the treatment. The DCE MRI images were then converted into concentration of gadolinium, and to calculate the area under the curve (AUC), the concentration was summed over a time course of 5 minutes with 6-second intervals.[51] The DCE MRI AUC data in the tumor was normalized to the DCE MRI AUC data in normal muscle tissues. For each time point, the means were computed for each mouse and then averaged among all mice.

The spectrum acquired with a 2-degree flip angle immediately before the 3D GRASE images was used to normalize the ^{13}C data. The ^{13}C pyruvate and lactate signals were normalized to the pyruvate signal from the spectrum, while the urea signal was normalized to the spectral urea signal. Only voxels with signal-to-noise ratios larger than 3 were considered. All voxels used to analyze a region were completely within the defined boundary (i.e. voxels on the boundary of the ablated region and the margin zone were not considered).

The means of the ^{13}C-labeled lactate, pyruvate, and urea imaging results as well as the DCE MRI AUC and K^{trans}, and the ADC, were calculated at baseline and each of the post-treatment follow-up time points. The significance of each of the post-HIFU time points compared to baseline was reported using the standard Mann-Whitney-Wilcoxon rank signed test, $p<0.05$.

Results

Small Animal FUS—Acoustic Characterization

Figure 2 shows the intensity beam plots of the coronal and axial cross sections of the focused ultrasound applicator beam pattern, as measured outside of the distal conical tip, and represents the portion to be positioned within the tumor. The full width half max of the coronal slice of the ultrasound beam was 0.8mm, and the 50% contour of the beam intensity extended 9mm from the surface of the cone. As measured by the radiation force balance, the acoustic efficiency of the ultrasound HIFU applicator ranged between 35–45%. The required applied power level to deliver the desired focal intensity for each animal experiment was scaled from the low power calibration measurements using this measured efficiency, with 11.6–15 W power delivery required to generate focal intensities of I_{SPTA} = 292.9–400.9W/cm^2 as in Table 1 for ablative doses of HIFU to be applied to the murine tumors.

With the narrow beam width and high intensity delivery, local ablation was effectively achieved in all five TRAMP mice.

Pathologic and Imaging Effects of HIFU

Figures 3 and 4 show representative sets of HP ^{13}C/mp-^{1}H MRI serial data with associated pathology from mice having 2.2cm^3 and 1.5cm^3 tumors treated with HIFU. The baseline HP ^{13}C lactate/pyruvate ratios were 3.01 ± 1.08 and 1.46 ± 0.63, indicating a range in metabolic activity consistent with varying pathologic grades of these tumors.[35] The baseline HP ^{13}C lactate/pyruvate and tumor volumes for all 5 mice studied (Table 1) demonstrate a range of cancer aggressiveness, from a ratio of 1.06 indicating a less aggressive tumor, to 3.01 as in a late-stage prostate tumor. In the ablated region 5 days after HIFU, both TTC (Figure 3a and 4a) and H&E staining (Figure 3b and 4b), Ki-67 (Figure 3c and 4c) and PIM (Figure 3d and 4d) demonstrated fragmented, non-viable cells consistent with coagulative necrosis.[15] In the partially treated tissue surrounding the ablated regions (margin zones) a mixture of destroyed tissue and viable cells were observed. As shown in Table 2, the viable cells were highly proliferative (mean Ki-67 staining 89.6% ± 4.3%). About 25% of the viable tumor was hypoxic (PIM staining positive for 25% ± 1.6% of the tumor) and were pathologically poorly differentiated (98.6% ± 1.0% of the tumor cells being poorly differentiated). The two mice had 1.1cm^3 and 0.6cm^3 ablated regions, respectively. The ablated and margin zones were then registered to the MRI T_2-weighted anatomical images (Figure 3e and 4e) in order to compare changes in measurements of metabolism (normalized HP ^{13}C lactate) and perfusion (normalized ^{13}C urea and DCE MRI). Figures 3e and 4e show representative imaging results at baseline, 3–4 hours, 1 day and 5 days post HIFU treatment. For both mice at baseline, normalized images of HP ^{13}C lactate and HP ^{13}C urea, DCE MRI AUC were heterogeneous in intensity but clearly observable throughout the TRAMP tumor consistent with viable metabolically active prostate cancer. Despite different HIFU doses applied in the two cases, a similar post-treatment tissue response was observed. In the pathologically ablated regions, the intensity of normalized HP ^{13}C lactate or HP ^{13}C urea and gadolinium AUC images were reduced to the level of the noise by 3 to 4 hours after treatment. Neither metabolism nor perfusion showed signs of recovery in the ablated regions by the 5-day time point in either case. In contrast, the partially treated zone had an initial decrease in metabolism (normalized lactate images) and perfusion (normalized urea and DCE MRI AUC images) 3–4 hours after treatment, followed by recovery back to or beyond baseline values by 5 days after treatment.

Figure 5 shows representative DCE MRI data in the margin zone of Mouse 2 treated with HIFU. The pre-treatment DCE MRI curve (blue) is consistent with the presence of high-grade prostate cancer: fast wash-in and fast wash-out of the gadolinium contrast agent.[52,53] At 3–4 hours after the treatment (red), the time to peak DCE MRI intensity is longer (200s vs. 100s), the plateau of the DCE intensity curve increased, and minimal contrast agent wash-out was observed. These changes are consistent with early vascular congestion and rupturing [54], and an increase in the extravascular, extracellular space volume fraction (v_e) from cell death due to the thermal dose delivered to this region. One day after the treatment (orange), the wash-in slope was still lower than the baseline values indicating the vasculature hadn't fully recovered. Five days after the treatment (green), both the wash-in and wash-out

slopes were higher than baseline, consistent with the pathologic finding of a poorly differentiated residual tumor (Table 2).

The compiled HP ^{13}C/mp-^{1}H MRI data from the 5 mice studied (Figure 6) quantitatively demonstrates the reproducibility of the significant loss of metabolism (HP ^{13}C lactate production) and perfusion (urea, DCE MRI and K^{trans}) at 3–4 hours after treatment in the ablated regions with no significant ($p = 0.31$) recovery by 5–6 days after treatment. In the tissues that received sub-lethal heat dose, there was a significant 60% ± 12.4% drop in HP ^{13}C lactate production and a significant 30 ± 13.7% drop in urea perfusion 3–4 hours after treatment, followed by recovery back to baseline by 5 days after treatment. DCE MRI K^{trans} and AUC showed a similar trend as the ^{13}C urea, having a complete loss of perfusion with no recovery in the ablated region while having a 40%–50% decrease 3–4 hours after treatment followed by recovery by 5 days.

The change in ADC was not significantly different from baseline versus time after HIFU treatment in either the ablated or margin regions. However, there was a trend for increasing ADC versus time in the ablated regions (% change from baseline being: −4% ± 12%, 13% ± 15%, 25% ± 17%, for 3–4 hours, 1 day and 5 days respectively). Whereas in the margin region, where there was recovery of tumor perfusion and metabolism, mean water ADC was variable with no net change by 5 days after treatment (7% ± 21%). The mean water ADC was non-significantly ($p= 0.16$) higher in the ablated (1.1×10^{-3} mm^2/sec) versus the partially treated zone (0.77×10^{-3} mm^2/sec). Additionally, tumor volume had a significant increase from baseline (a day before the treatment) to the day of the treatment (20% ± 4% increase from baseline), and then remained constant for the duration of the follow-up (21% ± 2% and 19% ± 5% for 1 and 5 days after treatment, respectively).

Discussion

The overall objective of this pre-clinical study was to develop HP ^{13}C MR biomarkers of prostate cancer ablation using HIFU, such that imaging at the time of treatment can be used to accurately predict the success and extent of coagulative ablation, and to identify tissues bordering the tumor that are potentially sensitized to adjuvant treatment (radiation, chemotherapy) by non-lethal hyperthermic heat doses. The ability to accurately predict the extent and success of HIFU ablation and tumor borders that have received sensitizing hyperthermic doses will be of vital importance in upcoming clinical trials of focal HIFU, both alone and in combination with adjuvant therapy in prostate cancer. To accomplish this goal a combined HP dual agent (^{13}C-pyruvate and ^{13}C-urea) ^{13}C MRI/mp-^{1}H MRI approach was used for the first time to establish early serial changes (3–4 hours up to 6 days) in perfusion and metabolism that occur in regions of HIFU ablation and adjacent partial treatment zones in the well-established TRAMP model.[37,41–43] In the ablated zone, the thermal insult was sufficient to cause complete cell death and coagulative necrosis, resulting in a complete loss of metabolism and perfusion by 3–4 hours after treatment without any recovery by 5 days. The loss of perfusion was demonstrated by a complete loss and lack of recovery of HP ^{13}C urea signal and water signal intensity on DCE MRI, and an associated loss of production in HP [1-^{13}C]lactate from HP [1-^{13}C]pyruvate. The loss of perfusion and metabolism in ablated regions were consistent across tumors of varying volume and

aggressiveness and the regions of loss of perfusion spatially correlated with lost metabolism. These findings are consistent with the presence of coagulative necrosis in the ablated regions. While prior ^{1}H MRI studies have not reported on changes in tumor metabolism after HIFU, the observed loss of perfusion in HIFU ablated tumors is consistent with prior contrast enhanced ^{1}H MRI studies. The loss of contrast agent enhancement in the ablated regions after focused ultrasound treatments has been demonstrated in patients with breast cancer [55] and liver metastases.[12] It is important to note that in this study neither tumor volume nor water ADC predicted effective ablation. Similar to prior publications we observed an early non-significant decrease in ADC, and a trend towards increasing water ADC over time in the ablated region.[56] Additionally, at 5 days after treatment the ADC was higher in the ablated zone than in the partially treated zone, consistent with the literature.[57] Tumor volume changes after HIFU are confounded by the fact that only part of the tumor was ablated in this study, and there was tumor growth in the partially treated regions as described below.

In contrast to the ablated region, partially treated tissues bordering the ablated region had a significant decrease in perfusion (HP ^{13}C urea and DCE MRI) and metabolism (HP ^{13}C lactate) 3–4 hours after treatment, followed by recovery of both perfusion and metabolism back to or beyond baseline values by 5 days after treatment. As compared to the ablated regions, there was much more variability in all of the imaging data in partially treated tumor regions; most likely due to the baseline pathologic heterogeneity of TRAMP tumors and differences in the thermal doses delivered. The time course of perfusion and metabolic recovery are consistent with the delivery of a reversible sub-lethal thermal dose; with histopathology, Ki-67 and PIM staining at 5 days after treatment indicating the recovery of proliferating, predominately poorly differentiated tumor cells, and levels of hypoxia consistent with baseline high-grade TRAMP tumors prior to treatment.[37] The early reduction of HP ^{13}C lactate production with effective cancer treatment has been shown in a number of HP ^{13}C MRI publications. Specifically, a reduction in HP [1-^{13}C]lactate signals have been observed in subcutaneous murine lymphoma tumors after chemotherapy[58], in a rat glioma tumor model after radiotherapy[59], and in a murine model of human breast adenocarcinoma following doxorubicin treatment.[60] Additionally the magnitude of HP ^{13}C lactate production at 5 days post treatment is also consistent with what has been reported in the literature for highly proliferative TRAMP tumors prior to treatment. [35,38,61] The early reduction in HP ^{13}C urea and its relationship to increased tumor hypoxia is consistent with a prior study that reported that reduced ^{13}C-urea AUC was associated with increased hypoxia in high-versus low-grade TRAMP tumors.[36] The clinical gold standard for measuring effective HIFU is DCE MRI, and the observed decrease in K^{trans} and DCE MRI AUC immediately after HIFU and its recovery days after treatment have repeatedly been demonstrated in other studies.[54,56,62] However, it is important to note that if follow-up HIFU is required to treat residual tumor after the initial DCE MRI, entrapped contrast agent within coagulated tissue regions could negatively impact the accuracy of the proton resonance frequency shift MR thermometry.[63–65] This study demonstrated that HP ^{13}C urea provides similar information about tumor perfusion after HIFU therapy as DCE MRI, however there were small differences in the magnitude of the decrease in these perfusion biomarkers as well the degree of their recovery. These differences are most likely due to the size difference

between gadolinium and urea molecules, and additional studies are needed to more fully understand the mechanism of these differences. More importantly, HP ^{13}C MRI can be repeated during the HIFU treatment process without impacting the MR thermometry measurements.

The understanding of temporal perfusion and metabolic changes in the partially treated zone could be important for determining the timing of adjuvant therapies such as chemotherapy and radiation. It has been shown that reduced perfusion can negatively affect the outcome of chemotherapy since a lower concentration of anticancer drugs would be delivered to the tumor.[66] In addition, the presence of oxygen is crucial for effective radiation treatment: reactive oxygen species in tissues cause oxidative damage in DNA, proteins, and lipids, mediating the cytotoxic effect through mechanisms such as DNA strand breaks, loss of protein function, and membrane damage.[67] Therefore hypoxic tumor regions are resistant to radiotherapy due to the lack of oxygen.[68] Increased cellular proliferation is also known to modulate therapeutic response with increased cellular proliferation being associated with more effective chemo- and radiation therapy. [69–71] Tumor hypoxia resulting from reduced perfusion and a reduction in HP [1-^{13}C]lactate production indicating reduced cellular proliferation observed in partially treated tumor tissue 3–4 hours after the HIFU treatment, both suggest that this would *not* be an optimum time for adjuvant treatment.[37,72] The recovery of perfusion, as indicated by the urea signal and DCE MRI AUC and K^{trans}, and increased proliferation based on a high rate of HP ^{13}C lactate production, suggests that subjecting the residual prostate cancer to adjuvant treatment at 5 days after the HIFU treatment would result in a better outcome.

Data gathered in this murine study provides the basis and preliminary data for future studies evaluating changes in perfusion and metabolism provided by HP ^{13}C urea and [1-^{13}C]pyruvate MRI in human clinical trials of HIFU therapy. A number of factors support the feasibility of clinically translating the findings of this pre-clinical study. HP [1-^{13}C]pyruvate is already FDA IND approved for use in prostate cancer patients[38], and the clinical translation of HP ^{13}C urea and its co-polarization with [1-^{13}C]pyruvate for combined metabolic and perfusion imaging after a singe injection of HP probes has been NIH funded and is in progress. Moreover, a Phase II clinical trial of prostate cancer patients prior to and after therapy demonstrated that both high-spatial (0.5 cc) and temporal resolution (2 sec.) 3D dynamic HP ^{13}C MRI data can be acquired from throughout the prostate in 47 seconds using a echo planar spectroscopic imaging (EPSI) sequence on a clinical 3T MRI.[39] The short HP ^{13}C MRI acquisition time combined with the fact that two HP probe injections within the same imaging exam has already been FDA IND approved offers the possibility of monitoring the effectiveness of HIFU ablation, i.e. complete loss of perfusion and metabolism, during the HIFU procedure. Additionally, the non-radioactive/ non-toxic nature of HP ^{13}C MRI allows for serial imaging of perfusion and metabolism in patients after HIFU treatment, thereby providing the ability to serially monitor these parameters in order to optimize the timing of adjuvant treatment of the sensitized regions of residual tumor as has been suggested in this pre-clinical study. Ultimately, patient studies are required to determine whether HP ^{13}C MRI of co-polarized [1-^{13}C]pyruvate ^{13}C urea can be performed at sufficient spatial resolution to monitor the effectiveness of HIFU ablation in real-time and to provide an assessment of the perfusion and metabolic status of residual

disease that was not effectively treated. The findings of this manuscript can be used as motivation for the FDA IND approval of such a clinical trial.

A limitation of this study was that MRI based temperature maps were not acquired in this study, so differences in the imaging parameters over time within the partially treated regions could not be related to thermal dose.[73,74] An ongoing hyperthermia study is investigating the dose related changes in metabolism and perfusion in TRAMP tumors by performing real-time temperature mapping at the time of treatment. Another limitation was that the first imaging follow-up time was 3–4 hours after treatment, not immediately after treatment, since mice were allowed to physiologically recover from treatment before being exposed to the lengthy mp-^{1}H MRI/HP ^{13}C MRI acquisition under anesthesia. In ongoing hyperthermia studies, fast ^{13}C MRI (< 1sec) after injection of co-polarized ^{13}C pyruvate and ^{13}C urea is being performed right after treatment, without the longer mp-^{1}H MRI exam.

Summary

In summary, this study demonstrated that in a single imaging acquisition after injection of co-polarized [1-^{13}C]pyruvate and ^{13}C-urea that the region of HIFU induced coagulative ablation can be identified by complete loss of perfusion and metabolism. Moreover, recovery of perfusion and metabolism over time in surrounding tissues, receiving non-lethal hyperthermic heat doses, can be measured, which may be useful for discerning the best time to apply adjuvant chemo- and radiation therapy. The utility of these HP ^{13}C MR measures of perfusion and metabolism in optimizing focal HIFU, either alone or in combination with adjuvant therapy, will need to be tested in future studies. The use of this HP dual agent ^{13}C MRI approach in patient HIFU studies in the near future is feasible due to HP ^{13}C pyruvate MRI already being used in patient studies [38,39], and funded clinical studies are working towards the use of HP ^{13}C urea in patients.

Acknowledgments

This project was supported by the NIH grant P41EB013598. Special thanks to Dr. Barbara Foster at Roswell Cancer Institute, Buffalo, NY, for supplying TRAMP mice for this study. The authors would also like to thank Subramaniam Sukumar and Mark Van Criekinge for technical support, and thank Cade Fox for figure editing.

Abbreviations

HP	Hyperpolarized
TRAMP	transgenic adenocarcinoma of mouse prostate
DCE	dynamic contrast-enhanced
AUC	area under the curve
HIFU	high-intensity focused ultrasound
FUS	focused ultrasound
mp	multiparametric

LDH	lactate dehydrogenase
ABS	acrylonitrile butadiene styrene
TTC	triphenyl tetrazolium chloride
PBS	phosphate-buffered saline
ADC	apparent diffusion coefficient

References

1. Cancer Facts & Figures 2017. Atlanta: American Cancer Society; 2017.
2. Chen RC, Basak R, Meyer AM, et al. Association Between Choice of Radical Prostatectomy, External Beam Radiotherapy, Brachytherapy, or Active Surveillance and Patient-Reported Quality of Life Among Men With Localized Prostate Cancer. JAMA. Mar 21; 2017 317(11):1141–1150. [PubMed: 28324092]
3. Serrell EC, Pitts D, Hayn M, Beaule L, Hansen MH, Sammon JD. Review of the comparative effectiveness of radical prostatectomy, radiation therapy, or expectant management of localized prostate cancer in registry data. Urol Oncol. Nov 6.2017
4. Jain AK, Ennis RD. Focal therapy, differential therapy, and radiation treatment for prostate cancer. Adv Urol. 2012; 2012:573193. [PubMed: 22666239]
5. Tay KJ, Schulman AA, Sze C, Tsivian E, Polascik TJ. New advances in focal therapy for early stage prostate cancer. Expert Rev Anticancer Ther. Aug; 2017 17(8):737–743. [PubMed: 28635336]
6. Woodrum DA, Kawashima A, Gorny KR, Mynderse LA. Prostate cancer: state of the art imaging and focal treatment. Clin Radiol. Aug; 2017 72(8):665–679. [PubMed: 28385253]
7. Mendhiratta, N, Taneja, SS. Focal Therapy for Prostate Cancer. In: Mydlo, JH, Godec, CJ, editors. Prostate Cancer: Science and Clincial Practice. 2. Elsevier Ltd; 2016.
8. Marien A, Gill I, Ukimura O, Betrouni N, Villers A. Target ablation--image-guided therapy in prostate cancer. Urol Oncol. Aug; 2014 32(6):912–923. [PubMed: 24411788]
9. Sivaraman A, Barret E. Focal Therapy for Prostate Cancer: An "A la Carte" Approach. Eur Urol. Jun; 2016 69(6):973–975. [PubMed: 26778462]
10. Cline HE, Hynynen K, Watkins RD, et al. Focused US system for MR imaging-guided tumor ablation. Radiology. Mar; 1995 194(3):731–737. [PubMed: 7862971]
11. Copelan A, Hartman J, Chehab M, Venkatesan AM. High-Intensity Focused Ultrasound: Current Status for Image-Guided Therapy. Semin Intervent Radiol. Dec; 2015 32(4):398–415. [PubMed: 26622104]
12. Kennedy JE. High-intensity focused ultrasound in the treatment of solid tumours. Nat Rev Cancer. Apr; 2005 5(4):321–327. [PubMed: 15776004]
13. Kennedy JE, Ter Haar GR, Cranston D. High intensity focused ultrasound: surgery of the future? Br J Radiol. Sep; 2003 76(909):590–599. [PubMed: 14500272]
14. Chu KF, Dupuy DE. Thermal ablation of tumours: biological mechanisms and advances in therapy. Nat Rev Cancer. Mar; 2014 14(3):199–208. [PubMed: 24561446]
15. Coad, JE. Practical Pathology Perspectives for Minimally Invasive Hyperthermic Medical Devices. SPIE; 23 February 2011; San Francisco, CA: 2011.
16. Wang Y, Wang W, Wang L, Wang J, Tang J. Ultrasound-guided high-intensity focused ultrasound treatment for abdominal wall endometriosis: preliminary results. Eur J Radiol. Jul; 2011 79(1):56–59. [PubMed: 20116953]
17. Orsi F, Monfardini L, Bonomo G, Krokidis M, Della Vigna P, Disalvatore D. Ultrasound guided high intensity focused ultrasound (USgHIFU) ablation for uterine fibroids: Do we need the microbubbles? Int J Hyperthermia. May; 2015 31(3):233–239. [PubMed: 25758436]
18. Zhou M, Chen JY, Tang LD, Chen WZ, Wang ZB. Ultrasound-guided high-intensity focused ultrasound ablation for adenomyosis: the clinical experience of a single center. Fertil Steril. Mar 1; 2011 95(3):900–905. [PubMed: 21067723]

19. Foley JL, Little JW, Starr FL 3rd, Frantz C, Vaezy S. Image-guided HIFU neurolysis of peripheral nerves to treat spasticity and pain. Ultrasound Med Biol. Sep; 2004 30(9):1199–1207. [PubMed: 15550323]
20. Jolesz FA. MRI-guided focused ultrasound surgery. Annu Rev Med. 2009; 60:417–430. [PubMed: 19630579]
21. Napoli A, Anzidei M, Ciolina F, et al. MR-guided high-intensity focused ultrasound: current status of an emerging technology. Cardiovasc Intervent Radiol. Oct; 2013 36(5):1190–1203. [PubMed: 23474917]
22. Ellis S, Rieke V, Kohi M, Westphalen AC. Clinical applications for magnetic resonance guided high intensity focused ultrasound (MRgHIFU): present and future. J Med Imaging Radiat Oncol. Aug; 2013 57(4):391–399. [PubMed: 23870333]
23. Pron G. Magnetic Resonance-Guided High-Intensity Focused Ultrasound (MRgHIFU) Treatment of Symptomatic Uterine Fibroids: An Evidence-Based Analysis. Ont Health Technol Assess Ser. 2015; 15(4):1–86.
24. Maloney E, Hwang JH. Emerging HIFU applications in cancer therapy. Int J Hyperthermia. May; 2015 31(3):302–309. [PubMed: 25367011]
25. Verma, S, Lamba, MAS, Vigneron, DB, Jung, A, Kurhanewicz, J. Multi-parametric Magnetic Resonance Imaging Approaches in Focal Prostate Cancer Therapy. In: Polascik, TJ, editor. Imaging and Focal Therapy of Early Prostate Cancer. USA: Springer; 2012.
26. Lewa CJ, Majewska Z. Temperature relationships of proton spin-lattice relaxation time T1 in biological tissues. Bull Cancer. 1980; 67(5):525–530. [PubMed: 6260272]
27. Kim YS. Advances in MR image-guided high-intensity focused ultrasound therapy. Int J Hyperthermia. May; 2015 31(3):225–232. [PubMed: 25373687]
28. Yiallouras C, Damianou C. Review of MRI positioning devices for guiding focused ultrasound systems. Int J Med Robot. Jun; 2015 11(2):247–255. [PubMed: 25045075]
29. Zini C, Hipp E, Thomas S, Napoli A, Catalano C, Oto A. Ultrasound- and MR-guided focused ultrasound surgery for prostate cancer. World J Radiol. Jun 28; 2012 4(6):247–252. [PubMed: 22778876]
30. Napoli A, Anzidei M, De Nunzio C, et al. Real-time magnetic resonance-guided high-intensity focused ultrasound focal therapy for localised prostate cancer: preliminary experience. Eur Urol. Feb; 2013 63(2):395–398. [PubMed: 23159454]
31. Chopra R. Transurethral MR-HIFU for the treatment of localized prostate cancer. J Ther Ultrasound. Dec.2015 2015(3Suppl 1):O59.
32. Aoyagia R, Nakamura H, Azuma T, et al. Localized elasticity measurement for detection of coagulation during HIFU therapy. Conf Proc IEEE Eng Med Biol Soc. 2013; 2013:6273–6276. [PubMed: 24111174]
33. Zhao WP, Chen JY, Chen WZ. Dynamic contrast-enhanced MRI serves as a predictor of HIFU treatment outcome for uterine fibroids with hyperintensity in T2-weighted images. Exp Ther Med. Jan; 2016 11(1):328–334. [PubMed: 26889263]
34. Kurhanewicz J, Vigneron DB, Brindle K, et al. Analysis of cancer metabolism by imaging hyperpolarized nuclei: prospects for translation to clinical research. Neoplasia. Feb; 2011 13(2): 81–97. [PubMed: 21403835]
35. Albers MJ, Bok R, Chen AP, et al. Hyperpolarized 13C lactate, pyruvate, and alanine: noninvasive biomarkers for prostate cancer detection and grading. Cancer Res. Oct 15; 2008 68(20):8607–8615. [PubMed: 18922937]
36. Keshari KR, Sriram R, Van Criekinge M, et al. Metabolic reprogramming and validation of hyperpolarized 13C lactate as a prostate cancer biomarker using a human prostate tissue slice culture bioreactor. Prostate. Aug; 2013 73(11):1171–1181. [PubMed: 23532911]
37. Chen HY, Larson PEZ, Bok RA, et al. Assessing Prostate Cancer Aggressiveness with Hyperpolarized Dual-Agent 3D Dynamic Imaging of Metabolism and Perfusion. Cancer Res. Jun 15; 2017 77(12):3207–3216. [PubMed: 28428273]
38. Nelson SJ, Kurhanewicz J, Vigneron DB, et al. Metabolic imaging of patients with prostate cancer using hyperpolarized [1-(1)(3)C]pyruvate. Sci Transl Med. Aug 14.2013 5(198):198ra108.

39. Aggarwal R, Vigneron DB, Kurhanewicz J. Hyperpolarized 1-[(13)C]-Pyruvate Magnetic Resonance Imaging Detects an Early Metabolic Response to Androgen Ablation Therapy in Prostate Cancer. Eur Urol. Dec; 2017 72(6):1028–1029. [PubMed: 28765011]
40. Wilson DM, Keshari KR, Larson PE, et al. Multi-compound polarization by DNP allows simultaneous assessment of multiple enzymatic activities in vivo. J Magn Reson. Jul; 2010 205(1): 141–147. [PubMed: 20478721]
41. Hurwitz AA, Foster BA, Allison JP, Greenberg NM, Kwon ED. The TRAMP mouse as a model for prostate cancer. Curr Protoc Immunol. Nov.2001 Chapter 20(Unit 20):25.
42. Greenberg NM, DeMayo F, Finegold MJ, et al. Prostate cancer in a transgenic mouse. Proc Natl Acad Sci U S A. Apr 11; 1995 92(8):3439–3443. [PubMed: 7724580]
43. Costello LC, Franklin RB, Zou J, et al. Human prostate cancer ZIP1/zinc/citrate genetic/metabolic relationship in the TRAMP prostate cancer animal model. Cancer Biol Ther. Dec 15; 2011 12(12): 1078–1084. [PubMed: 22156800]
44. von Morze C, Larson PE, Hu S, et al. Imaging of blood flow using hyperpolarized [(13)C]urea in preclinical cancer models. J Magn Reson Imaging. Mar; 2011 33(3):692–697. [PubMed: 21563254]
45. Sukumar, S; Keshari, KR; Bok, R; , et al. Single-shot Frequency and Time Specific, 3D Imaging Method for Measuring Hyperpolarized 13C Biomarkers In-Viovo at 14.1 Tesla. Paper presented at: The International Society for Magnetic Resonance in Medicine2011;; Montreal, Quebec, Canada.
46. Beatty, CJ; Thomsen, SL; Vos, J; Coad, J. Practical pathology for thermal tissue applications. Paper presented at: SPIE; 11 March 2015, 2015; San Franciaco, CA.
47. Fedorov A, Beichel R, Kalpathy-Cramer J, et al. 3D Slicer as an image computing platform for the Quantitative Imaging Network. Magn Reson Imaging. Nov; 2012 30(9):1323–1341. [PubMed: 22770690]
48. Tofts PS, Kermode AG. Measurement of the Blood-Brain-Barrier Permeability and Leakage Space Using Dynamic Mr Imaging. 1. Fundamental-Concepts. Magnet Reson Med. Feb; 1991 17(2): 357–367.
49. Pickup S, Zhou R, Glickson J. MRI estimation of the arterial input function in mice. Acad Radiol. Sep; 2003 10(9):963–968. [PubMed: 13678084]
50. R: A language and environment for statistical computing [computer program]. Vienna, Austria: R Foundation for Statistical Computing; 2015.
51. Buckley, DL, Parker, GJM. Dynamic Contrast-Enhanced Magnetic Resonance Imaging in Oncology. Springer; Berlin Heidelberg: 2005. Measuring Contrast Agent Concentration in T1-Weighted Dynamic Contrast-Enhanced MRI; 69–79.
52. Chen YJ, Chu WC, Pu YS, Chueh SC, Shun CT, Tseng WY. Washout gradient in dynamic contrast-enhanced MRI is associated with tumor aggressiveness of prostate cancer. J Magn Reson Imaging. Oct; 2012 36(4):912–919. [PubMed: 22711415]
53. Kim JK, Hong SS, Choi YJ, et al. Wash-in rate on the basis of dynamic contrast-enhanced MRI: usefulness for prostate cancer detection and localization. J Magn Reson Imaging. Nov; 2005 22(5): 639–646. [PubMed: 16200542]
54. Cheng HLM, Purcell CM, Bilbao JM, Plewes DB. Prediction of subtle thermal histopathological change using a novel analysis of Gd-DTPA kinetics. J Magn Reson Imaging. Nov; 2003 18(5): 585–598. [PubMed: 14579402]
55. Furusawa H, Namba K, Thomsen S, et al. Magnetic resonance-guided focused ultrasound surgery of breast cancer: reliability and effectiveness. J Am Coll Surg. Jul; 2006 203(1):54–63. [PubMed: 16798487]
56. Hectors SJ, Jacobs I, Heijman E, et al. Multiparametric MRI analysis for the evaluation of MR-guided high intensity focused ultrasound tumor treatment. NMR Biomed. Sep; 2015 28(9):1125–1140. [PubMed: 26198899]
57. Kim KW, Lee JY, Lee JM, Jeon YS, Choi YS, Park J, Kim H, Han JK, Choi BI. High-intensity Focused Ultrasound Ablation of Soft-tissue Tumors and Assessment of Treatment Response with Multiparametric Magnetic Resonance Imaging: Preliminary Study Using Rabbit VX2 Tumor Model. J Med Ultrasound. 2014; 22(2):99–105.

58. Day SE, Kettunen MI, Gallagher FA, et al. Detecting tumor response to treatment using hyperpolarized 13C magnetic resonance imaging and spectroscopy. Nat Med. Nov; 2007 13(11): 1382–1387. [PubMed: 17965722]
59. Day SE, Kettunen MI, Cherukuri MK, et al. Detecting response of rat C6 glioma tumors to radiotherapy using hyperpolarized [1- 13C]pyruvate and 13C magnetic resonance spectroscopic imaging. Magn Reson Med. Feb; 2011 65(2):557–563. [PubMed: 21264939]
60. Witney TH, Kettunen MI, Hu DE, et al. Detecting treatment response in a model of human breast adenocarcinoma using hyperpolarised [1-13C]pyruvate and [1,4-13C2]fumarate. Br J Cancer. Oct 26; 2010 103(9):1400–1406. [PubMed: 20924379]
61. Golman K, Zandt RI, Lerche M, Pehrson R, Ardenkjaer-Larsen JH. Metabolic imaging by hyperpolarized 13C magnetic resonance imaging for in vivo tumor diagnosis. Cancer Res. Nov 15; 2006 66(22):10855–10860. [PubMed: 17108122]
62. Hijnen NM, Heijman E, Kohler MO, et al. Tumour hyperthermia and ablation in rats using a clinical MR-HIFU system equipped with a dedicated small animal set-up. Int J Hyperthermia. 2012; 28(2):141–155. [PubMed: 22335228]
63. Hijnen NM, Elevelt A, Grull H. Stability and trapping of magnetic resonance imaging contrast agents during high-intensity focused ultrasound ablation therapy. Invest Radiol. Jul; 2013 48(7): 517–524. [PubMed: 23695082]
64. Hijnen NM, Elevelt A, Pikkemaat J, Bos C, Bartels LW, Grull H. The magnetic susceptibility effect of gadolinium-based contrast agents on PRFS-based MR thermometry during thermal interventions. J Ther Ultrasound. 2013; 1:8. [PubMed: 25516799]
65. Staruch RM, Nofiele J, Walker J, et al. Assessment of acute thermal damage volumes in muscle using magnetization-prepared 3D T2 -weighted imaging following MRI-guided high-intensity focused ultrasound therapy. J Magn Reson Imaging. Aug; 2017 46(2):354–364. [PubMed: 28067975]
66. Yasuda H. Solid tumor physiology and hypoxia-induced chemo/radio-resistance: Novel strategy for cancer therapy: Nitric oxide donor as a therapeutic enhancer. Nitric Oxide-Biology and Chemistry. Sep; 2008 19(2):205–216. [PubMed: 18503779]
67. Wilson DM, Kurhanewicz J. Hyperpolarized 13C MR for molecular imaging of prostate cancer. J Nucl Med. Oct; 2014 55(10):1567–1572. [PubMed: 25168625]
68. Matsuo M, Matsumoto S, Mitchell JB, Krishna MC, Camphausen K. Magnetic resonance imaging of the tumor microenvironment in radiotherapy: perfusion, hypoxia, and metabolism. Semin Radiat Oncol. Jul; 2014 24(3):210–217. [PubMed: 24931096]
69. Amadori D, Volpi A, Maltoni R, et al. Cell proliferation as a predictor of response to chemotherapy in metastatic breast cancer: a prospective study. Breast Cancer Res Treat. Mar; 1997 43(1):7–14. [PubMed: 9065594]
70. Fowler JF, Ritter MA. A rationale for fractionation for slowly proliferating tumors such as prostatic adenocarcinoma. Int J Radiat Oncol Biol Phys. May 15; 1995 32(2):521–529. [PubMed: 7751194]
71. Hegemann NS, Guckenberger M, Belka C, Ganswindt U, Manapov F, Li M. Hypofractionated radiotherapy for prostate cancer. Radiat Oncol. Dec 6.2014 9:275. [PubMed: 25480014]
72. Chaplin DJ, Olive PL, Durand RE. Intermittent blood flow in a murine tumor: radiobiological effects. Cancer Res. Jan 15; 1987 47(2):597–601. [PubMed: 3791244]
73. Hazle JD, Diederich CJ, Kangasniemi M, Price RE, Olsson LE, Stafford RJ. MRI-guided thermal therapy of transplanted tumors in the canine prostate using a directional transurethral ultrasound applicator. J Magn Reson Imaging. Apr; 2002 15(4):409–417. [PubMed: 11948830]
74. Rieke V, Butts Pauly K. MR thermometry. J Magn Reson Imaging. Feb; 2008 27(2):376–390. [PubMed: 18219673]

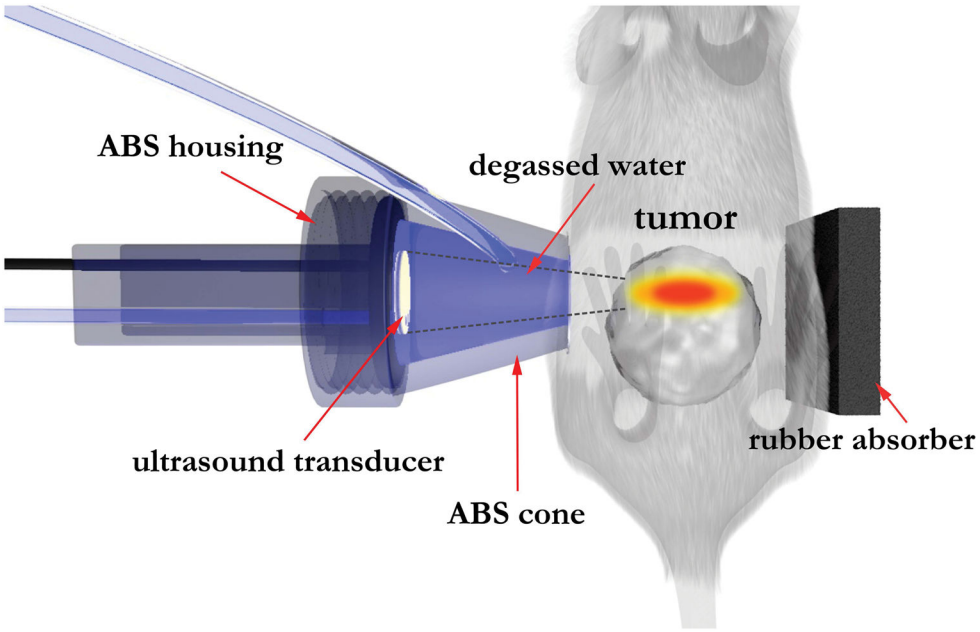

Figure 1.

Diagram showing the setup used for HIFU treatment of TRAMP tumors. The cone of the focused ultrasound applicator was filled with degassed water to adjust the depth such that the focal zone fell within the tumor. The ultrasound power and duration (Table 1) were adjusted to produce regions of ablation and partial treatment in all five TRAMP mice treated. The rubber absorber was positioned to absorb and dissipate the leftover ultrasound energy, and prevent reflections. Acoustic gel was applied at the interface between the mouse and the cone, and between the mouse and the rubber absorber.

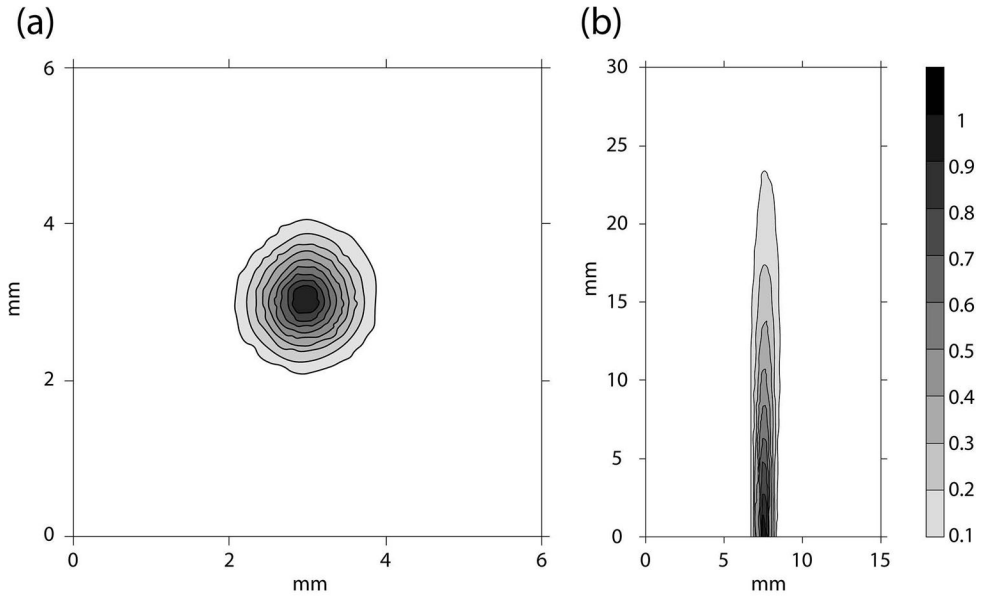

Figure 2.

The (a) transverse (4mm from the cone surface) and (b) axial cross-sections (starting from 2mm from the cone surface) of the ultrasound beam mapped out with a hydrophone in degassed water. The beam plots were performed with the cone attached (Figure 1). As shown in (b), the focal zone was adjusted such that it was near the surface of the cone where the top of the tumor would be positioned.

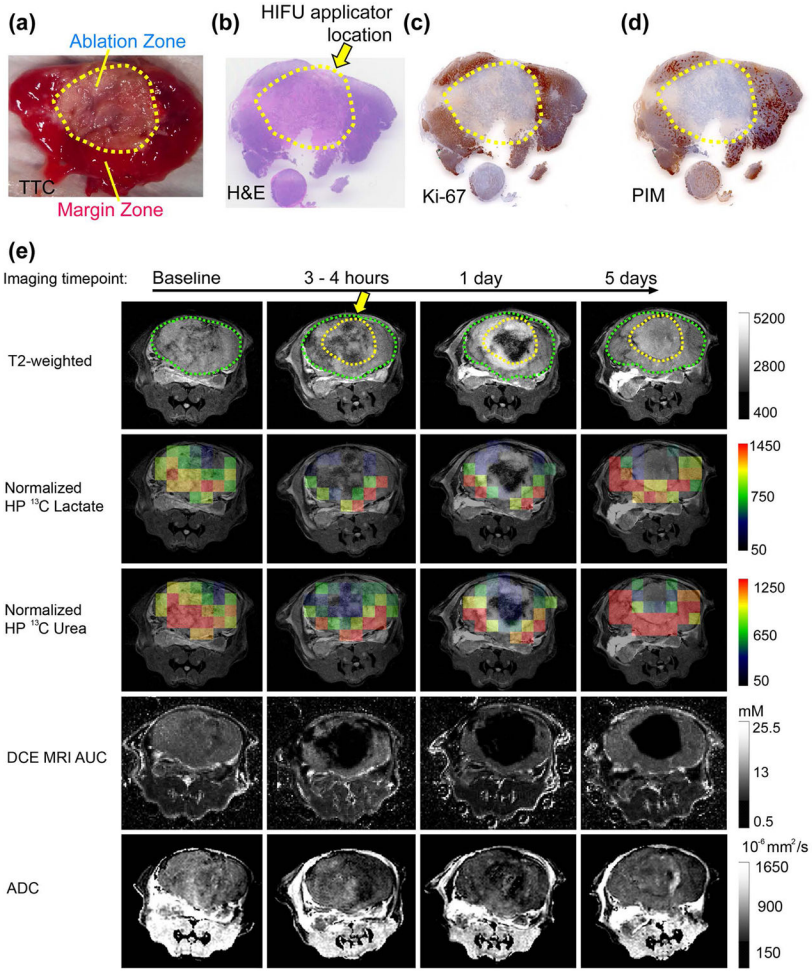

Figure 3.

Representative (a) TTC, (b) H&E, (c) Ki-67, and (d) PIM stained pathologic sections, and (e) the corresponding T2 weighted images, overlaid HP ^{13}C lactate, ^{13}C urea images on the T2 weighted images, DCE MRI AUC, and ADC of a large aggressive TRAMP tumor (Mouse 3). The position of the HIFU applicator is indicated by the yellow arrow. The region of ablation is demarcated by a dashed yellow line, and the outline of the TRAMP tumor is demarcated by the dashed green line. The margin zone was the region between the yellow and green lines.

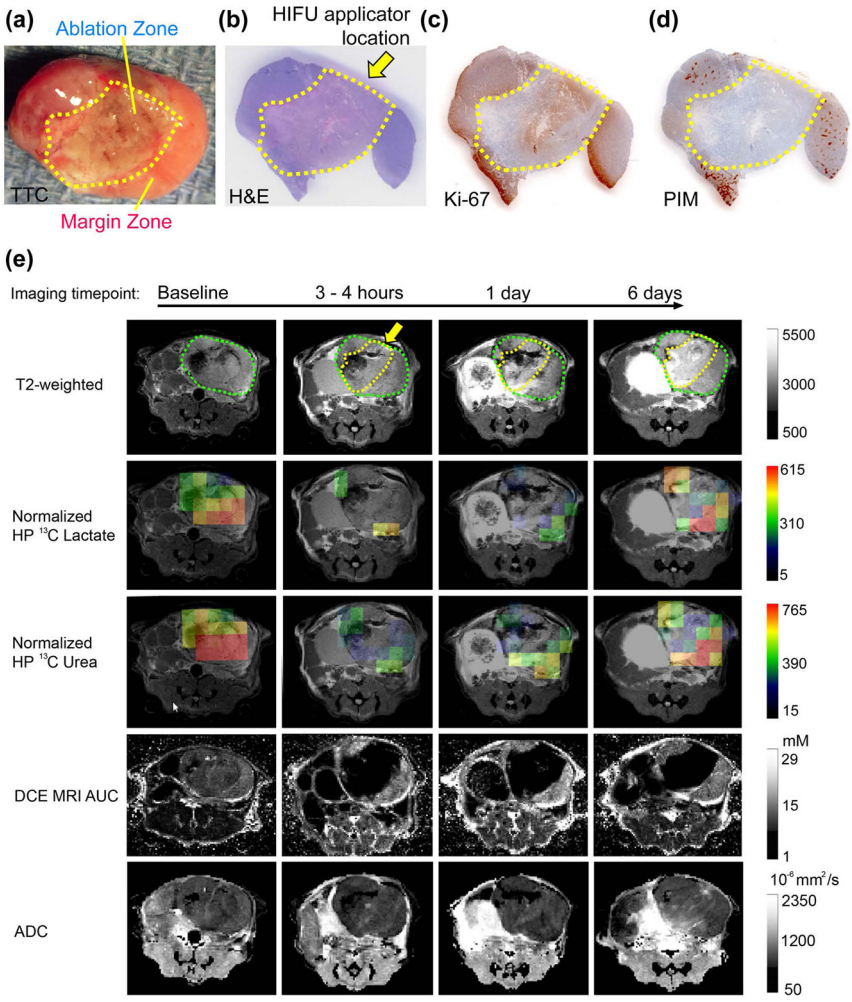

Figure 4.

Representative (a) TTC, (b) H&E, (c) Ki-67, and (d) PIM stained pathologic sections, and (e) the corresponding T2 weighted images, overlaid HP ^{13}C lactate, ^{13}C urea images on the T2 weighted images, DCE MRI AUC, and ADC of a smaller, less aggressive TRAMP tumor (Mouse 4). The position of the HIFU applicator is indicated by the yellow arrow. The region of ablation is demarcated by a dashed yellow line, and the outline of the TRAMP tumor is demarcated by the dashed green line. The margin zone was the region between the yellow and green lines.

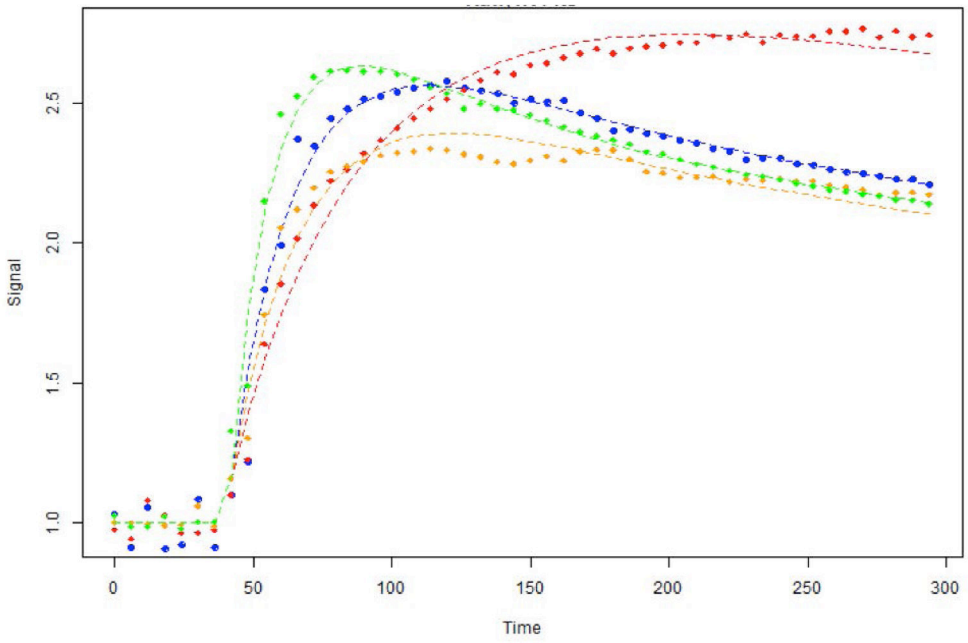

Figure 5.

These representative DCE MRI curves from Mouse 2 at baseline (blue), 3–4 hours after treatment (red), 1 (yellow) and 5 (green) days after HIFU treatment. The y-axis is the signal intensity over the average of the pre-contrast enhanced baselines (the first six time points.)

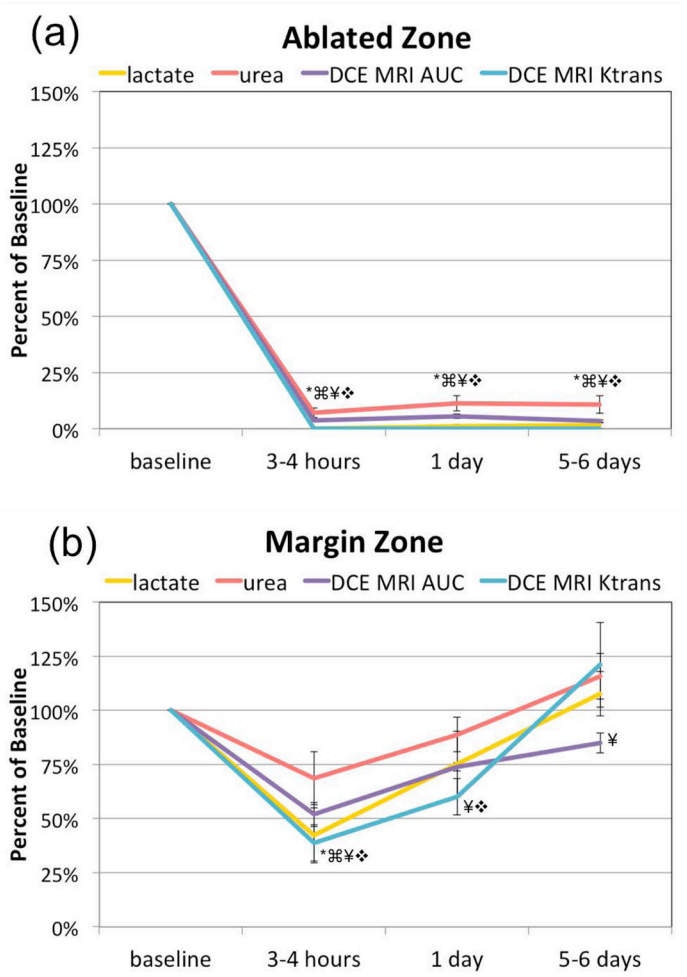

Figure 6.

A graphical summary of the means ± stand errors change of baseline of HP ^{13}C urea, [1-^{13}C] lactate, DCE MRI AUC, and K^{trans} in the ablated (a) and margin (b) zones of the TRAMP tumor after HIFU treatment. Statistically significant changes ($p < 0.05$) compared to baseline are indicated by the following symbols: * for lactate, ⌘ for urea, ¥ for DCE MRI AUC, and ❖ for K^{trans}.

Table 1

Summary of the tumor volumes, baseline tumor lactate-to-pyruvate ratio (an indicator for tumor aggressiveness), treatment parameters (power and duration), and ablated volumes in the five mice studied.

Mouse #	Tumor Volume (cm^3)	Lac/Pyr	Number of Sonications	Input Power (W)	I_{SPTA} ($W/cm^{2)}$	Duration (s/sonication)	Estimated % of tumor ablated
1	2.039	1.06±0.77	1	15	400.92	90	50%
2	1.759	2.28±0.60	2	12	303.00	60	35%
3	2.225	3.01±1.08	2	12	303.00	60	50%
4	1.485	1.46±0.63	2	12	303.00	45	40%
5	2.037	2.38±1.23	2	11.6	292.90	45	20%

Table 2

The histology readings of H&E, Ki-67, and PIM of the partially treated zones of all five mice after the 5-day imaging time point.

	H&E (%)			
Mouse #	**Poorly differentiated**	**Well differentiated**	**Ki-67(% stained)**	**PIM(% stained)**
1	100	0	95	30
2	100	0	95	20
3	95	5	98	25
4	100	0	95	30
5	98	2	75	25